PERGAMON

Computers and Structures 73 (1999) 425–435

Computers & Structures

www.elsevier.com/locate/compstruc

Incremental analysis of time-dependent effects in composite structures

Bruno Jurkiewiez[a], Jean-François Destrebecq[b,*], Alain Vergne[b]

[a]LERGEC, University Robert Schuman, Strasbourg, IUT Strasbourg-sud, 72 route du Rhin, F-67400, Illkirch, France
[b]LERMES, University Blaise Pascal, Clermont-Ferrand, CUST, BP 206, F-63174, Aubiere, France

Received 8 November 1996; accepted 2 October 1998

Abstract

An efficient numerical method is presented, to account for time effects in composite structures. The method is based on the theory of linear viscoelasticity and on the finite element method. The global behaviour of structural elements made of several viscoelastic materials (composite beams, layered plates or shells) is expressed in terms of the generalized variables of the structure mechanics. The incremental nature of the formulation results from the choice of a Dirichlet's series to express the constitutive law of the materials. A specific algorithm which allows for a process of construction by phases is implemented in a finite element program. The use of the method is illustrated through two computation examples: a prestressed concrete beam previously tested over a 5-year period of creeping, and an existing cooling tower which is a thin reinforced concrete shell. The method provides valuable information about time effects that may be used either while designing new structures, or for the diagnosis of existing structures.

Keywords: Creep; Shrinkage; Viscoelasticity; Composite structures; Finite element method

1. Introduction

Concrete, wood, bituminous materials, etc. are widely used in building technology. The behaviour of such materials is usually time-dependent. As a major consequence, a stress and strain redistribution is commonly observed, along with a significant increase in deflections and displacements of the structures under service conditions. Taking advantage of the constant progress in computing science and facilities, engineers feel more and more concerned with the necessity of achieving a fair estimation of such effects, either for pure design purposes, or for the diagnosis of existing structures.

The main purpose of our research work is to investigate reliable and efficient improvements in numerical methods, that may be used for the time analysis of building structures. The step-by-step computation method presented below is based on the theory of linear viscoelasticity and on the finite element method. It applies to the analysis of structures made of composite elements such as composite beams, layered plates or shells. The use of the method is illustrated by two practical examples.

2. Accounting for time-dependent behaviour of building materials

Creep, relaxation and shrinkage are time-related

* Corresponding author.

0045-7949/99/$ - see front matter
PII: S0045-7949(98)00269-7

phenomena that may affect the mechanical behaviour of normal materials under service load conditions:

- creep is a progressive increase in strain under sustained loading (Fig. 1);
- relaxation is the dual phenomenon; it corresponds to a stress decrease under constant strain conditions;
- shrinkage is a volumetric self-contraction of the unconstrained material.

For building materials such as concrete and wood, creep (or relaxation) and shrinkage are usually described as a combination of an autogenous behaviour (known as basic creep or basic shrinkage) and a drying phenomenon caused by a water loss to the ambient atmosphere. From a physical point of view, the theory of linear viscoelasticity may not be fully adequate to describe time-dependent phenomena in the behaviour of building materials. It is commonly accepted that the theory of linear viscoelasticity applies to the basic creep of such materials. The extension of this theory to drying creep or relaxation is more questionable. During the drying process, the creep rate depends on the moisture content in the material. Limited damage or fracture effects may also develop in the same time. In practice, these phenomena may be accounted for by expressing the creep or relaxation law with regards to the member size and to the ambient conditions. Laws proposed by Eurocode 2 [1,2] for the time-dependent behaviour of concrete (creep and shrinkage) depend on these two parameters, on the concrete mix and on the age at loading time. Based on such adjusted laws, the theory of linear viscoelasticity may be accepted as sufficient for design purposes of engineering structures under service conditions (normal temperature, low stress level) [3].

In prestressing devices, the loss of tension is progressive and limited in range. Therefore, we may assume that the same theory will provide a satisfactory approximation of prestressing stress relaxation.

2.1. Integral approach

The theory of linear viscoelasticity is based on Boltzmann's superposition principle. According to this theory, the constitutive law of the material may be expressed as a Volterra's integral equation [4]:

$$\forall t \geq t_0: \quad \epsilon(t) = J(t,t)\sigma(t) - \int_{t_0}^{t} \frac{\partial J(t,\tau)}{\partial \tau}\sigma(\tau)\,\mathrm{d}\tau \tag{1}$$

where t_0 is the time at first loading. In this equation, $\sigma(t)$ and $\epsilon(t)$ denote the stress and strain at any time t. In a general approach, the creep function $J(t,t_0)$ depends on both the time at loading t_0 and the actual time t. Creep function and relaxation function are dual. From Eq. (1), it can be shown that they satisfy the following equation:

$$\forall t \geq t_0 \quad J(t,t)R(t,t_0) - \int_{t_0}^{t} \frac{\partial J(t,\tau)}{\partial \tau}R(\tau,t_0)\,\mathrm{d}\tau = 1 \tag{2}$$

where $R(t,t_0)$ is the relaxation function of the material. When only one of the two functions is known, the other can be determined by solving Eq. (2).

Eq. (1) can be used for the time analysis of viscoelastic structures. In order to solve the integral equation, the life-span $[t_0,t]$ must be divided into a number of finite intervals. Thus, the calculation can be performed as a step-by-step procedure. Such an approach requires the stress history $\sigma(\tau)$ to be stored at any intermediate step of time over the whole life-span of the structure. As a consequence, a large memory size is required and the computation process is time consuming. This method is hardly suited for the analysis of huge or complicated structures.

2.2. Incremental approach

An alternative way to account for the viscoelastic behaviour of materials is to expand the characteristic function, namely the creep function or the relaxation function, into a Dirichlet series. In the latter case, the relaxation function is expressed as a sum of decaying exponential terms:

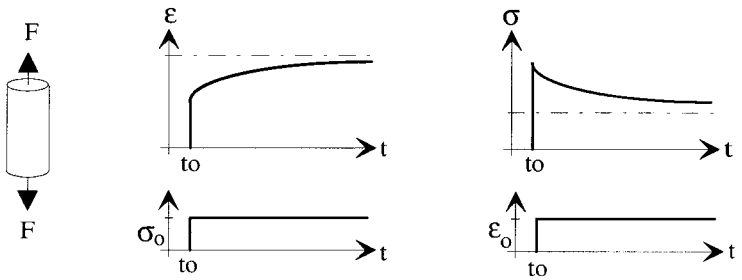

Fig. 1. Creep and relaxation behaviour of a viscoelastic material.

$$R(t,t_0) = E_0(t_0) + \sum_{\mu=1}^{r} E_\mu(t_0)\mathrm{e}^{-\lambda_\mu(t-t_0)} \tag{3}$$

where λ_μ^{-1} is called the relaxation time. This approach has been carefully investigated by Bazant and Wu [5] in the case of a time hardening material such as concrete. By analogy with a generalized Maxwell's model, they proposed that the constitutive law of a viscoelastic material should be represented by a set of linear differential equations:

$$\dot{\sigma}_\mu(t) + \lambda_\mu\sigma_\mu(t) = E_\mu(t)\big(\dot{\epsilon}(t) - \dot{\epsilon}^*(t)\big) \quad \mu = 0,\ldots,r \tag{4}$$

where

$$\lambda_0 = 0$$

and

$$\sigma(t) = \sum_{\mu=0}^{r}\sigma_\mu(t)\ \forall t$$

$\sigma_\mu(t)$ represents a set of $r+1$ internal variables, each of them being attached to the corresponding μ-branch of the Maxwell's model. $\epsilon^*(t)$ represents any given stress-independent strain, such as shrinkage or temperature induced strain. The solution of the system of differential equations shown above (Eq. (4)) can be expressed as an incremental expression for any finite time interval $[t,t+\Delta t]$:

$$\forall t,\Delta t:\quad \Delta\sigma = \tilde{E}(t)\Delta\epsilon + \sigma^{\mathrm{his}}(t) - \Delta\sigma^* \tag{5}$$

where $\Delta\sigma^* = \tilde{E}(t)\Delta\epsilon^*$, $\Delta\epsilon^*$ being the increase in $\epsilon^*(t)$ during the time interval Δt. $\tilde{E}(t)$ is a fictitious modulus whose value depends on t and Δt. $\sigma^{\mathrm{his}}(t)$ accounts for the whole stress history since the beginning of the loading period. It depends on the actual values of the cumulative variables $\sigma_\mu(t)$ at the beginning of the specified step of time:

$$\sigma^{\mathrm{his}}(t) = -\sum_{\mu=1}^{r}\sigma_\mu(t)\,(1-\mathrm{e}^{-\lambda_\mu\Delta t}) \tag{6}$$

The incremental formulation (Eq. (5)) may be generalized for a two-dimensional isotropic material. Under the hypothesis that the Poisson's ratio remains equal to its initial value ν, it yields:

$$\forall t,\Delta t:\quad \{\Delta\sigma\} = [\nu]\big(\tilde{E}(t)\{\Delta\epsilon\} + \{\sigma^{\mathrm{his}}(t)\} - \{\Delta\sigma^*\}\big) \tag{7}$$

where

$$[\nu] = \frac{1}{1-\nu^2}\begin{bmatrix} 1 & \nu & 0 \\ \nu & 1 & 0 \\ 0 & 0 & \dfrac{1-\nu}{2} \end{bmatrix}$$

2.3. Law calibration

It may occur that only the creep function of the material is known. In that case, the relaxation function must be derived from the creep function by solving Eq. (2) numerically. Let the time period $[t_0,t]$ be divided into k finite intervals. For every time interval, the creep function and the relaxation function are assumed to approximate to linear variations. Thus, the relaxation function may be calculated step-by-step by increasing k in the following formula:

$\forall k \geq 1$

$$R_{k,0} = \frac{2 + R_{0,0}(J_{k,0} - J_{k,1}) + \sum_{j=1}^{k-1} R_{j,0}(J_{k,j-1} - J_{k,j+1})}{J_{k,k-1} + J_{k,k}} \tag{8}$$

where $t_k = t$, $J_{k,i} = J(t_k,t_i)$, $R_{j,0} = R(t_j,t_0)$ and $R_{0,0} = R(t_0,t_0) = E(t_0)$, $E(t_0)$ being the modulus of elasticity of the material at time t_0.

When the relaxation function is known, the law calibration consists in adjusting a Dirichlet series (defined above by Eq. (3)) in order to fit the relaxation function. A least square method is used to determine the $E_\mu(t_0)$ parameters, the time of relaxation λ_μ^{-1} having been given suitable values.

An acceptable accuracy is usually achieved by fixing a number of branches in the Maxwell chain equal to $r = 4$. In the case of a time hardening material (concrete for example), the procedure is repeated for increasing values of the initial time t_0, the λ_μ parameters being kept constant. The effect of time on the $E_\mu(t_0)$ parameters is accounted for by another Dirichlet series:

$$E_\mu(t_0) = \sum_{s=1}^{3}\Gamma_{\mu,s}\mathrm{e}^{-\gamma_s t_0} \quad \mu = 0,\ldots,r \tag{9}$$

where γ_s parameters have fixed values. The $\Gamma_{\mu,s}$ coefficients are also determined by a least square method. The whole law calibration procedure must be processed before any application, by running a specific routine specially written for this purpose.

3. A global approach for the analysis of viscoelastic structures

Eq. (5) or (7) may be regarded as an expression of the constitutive law of an elastic body subjected to initial stress conditions. This formulation can be implemented in any finite element program suitable for

Table 1

Composite beam	Layered iostropic shell
Generalized stresses and strains	
$\{S\} = \begin{Bmatrix} N \\ M \end{Bmatrix}$	$\{S\} = \begin{Bmatrix} \{N\} \\ \{M\} \end{Bmatrix}$
$\{D\} = \begin{Bmatrix} \epsilon_0 \\ \chi \end{Bmatrix}$	$\{S\} = \begin{Bmatrix} \{\epsilon_0\} \\ \{\chi\} \end{Bmatrix}$
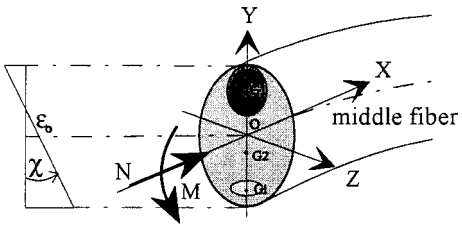	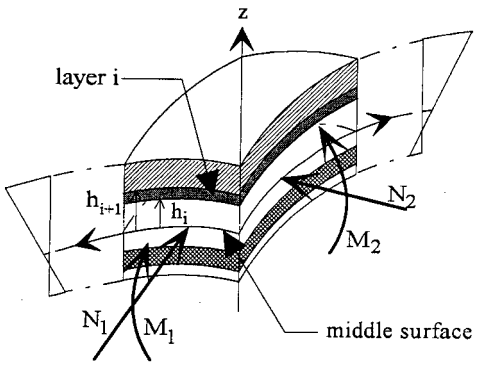
Global stiffness matrix	
$[\tilde{H}(t)] = \sum_{i=1}^{n} \tilde{E}_i(t) \begin{Bmatrix} -\Omega_i & y_{Gi}\Omega_i \\ y_{Gi}\Omega_i & -I_i \end{Bmatrix}$	$[\tilde{H}(t)] = \sum_{i=1}^{n} \tilde{E}_i(t)[v]_i \begin{Bmatrix} (h_{i+1} - h_i) & (h_{i+1}^2 - h_i^2)/2 \\ (h_{i+1}^2 - h_i^2)/2 & (h_{i+1}^3 - h_i^3)/3 \end{Bmatrix}$
Generalized stresses due to load history and free dilatation	
$\{S^{\text{his}}(t)\} = \sum_{i=1}^{n} \int_{\Omega_i} \begin{Bmatrix} -1 \\ y \end{Bmatrix} \sigma_i^{\text{his}}(t) \mathrm{d}\Omega$	$\{S^{\text{his}}(t)\} = \sum_{i=1}^{n} [v]_i \int_{h_i}^{h_{i+1}} \begin{Bmatrix} \{\sigma^{\text{his}}(t)\}_i \\ z\{\sigma^{\text{his}}(t)\}_i \end{Bmatrix} \mathrm{d}z$
$\{\Delta S^*\} = \sum_{i=1}^{n} \int_{\Omega_i} \begin{Bmatrix} -1 \\ y \end{Bmatrix} \Delta\sigma_i^* \mathrm{d}\Omega$	$\{\Delta S^*\} = \sum_{i=1}^{n} [v]_i \int_{h_i}^{h_{i+1}} \begin{Bmatrix} \{\Delta\sigma^*\}_i \\ z\{\Delta\sigma^*\}_i \end{Bmatrix} \mathrm{d}z$

elastic structure design. The time analysis must be performed as a step-by-step procedure, in order to scan the life-span of the structure. The set of cumulative variables attached to every finite element (see Eq. (6)) must be updated at the end of every computation step. Such an approach may be both time and memory consuming, especially in the case of a huge structure.

In order to decrease the number of degrees of freedom, thus to make the computation process faster, we propose expressing the time dependent behaviour of structural elements in terms of the generalized strains (denoted below as $\{D(t)\}$) versus the generalized stresses (denoted below as $\{S(t)\}$). The principle of this approach is to include the behaviour of the constituent materials, as expressed by Eq. (5) or (7), in the classic theories of beams, plates or shells. This approach yields an incremental relationship for the behaviour of the cross-section of the specified structural element during the time interval $[t,t+\Delta t]$:

$$\{\Delta S\} = \left[\tilde{H}(t)\right]\{\Delta D\} + \left\{S^{\text{his}}(t)\right\} - \{\Delta S^*\} \tag{10}$$

The meaning of each term of this equation is shown in Table 1 in the case of a composite beam and in the case of a thin layered isotropic shell. In both cases, the structural elements are made of n elastic or viscoelastic zones, with a full connection between zones. The time dependent behaviour of each zone is defined by Eq. (5) or (7), respectively. The formulae for a layered isotro-

pic plate may be derived from the case of the shell by giving the curvature radii infinite values.

The generalized stress $\{S(t)\}$ is composed of normal/shear forces and bending/twisting moments. The generalized strain $\{D(t)\}$ consists of axial strain components $\{\epsilon\}$ and curvature components $\{\chi\}$. $[\tilde{H}(t)]$ is a fictitious stiffness matrix which depends on the composition of the element, on the actual time t and on the time interval Δt. This matrix includes extra-diagonal terms that show a coupling effect between axial and bending variables.

The actual value of $\sigma^{\text{his}}(t)$ depends in a linear way on the previous values of the normal stress at any given location within the cross-section of the element. As a consequence, it may be shown that the distribution of $\sigma^{\text{his}}(t)$ is linear throughout each elementary zone of the composite beam or the layered shell or plate. Although the distribution of $\epsilon^*(t)$, therefore $\sigma^*(t)$, might be non-linear, it is generally assumed linearly distributed in practice. The hypothesis of a linear distribution makes the calculation of $\{S^{\text{his}}(t)\}$ and $\{\Delta S^*\}$ easier.

4. Implementation in a finite element program

In order to implement our approach, the finite element method has been chosen because it allows a large range of various problems to be solved. As a matter of fact, problems to be solved may be expressed either in terms of the local variables σ–ϵ, or in terms of the generalized variables of the beam, plate or shell theories.

4.1. The step-by-step procedure

As shown above, the incremental approach yields a formulation similar to linear elasticity with initial stress (Eq. (5) or (7)). The incremental nature of this formulation requires the computation to be conducted step-by-step. An instant loading of the structure corresponds to an elastic calculation step. If the external load is kept constant over a time interval $[t,t+\Delta t]$, the increase in the virtual work Δw is given by the work increase Δw^{int} produced by the internal forces σ^{his} and $\Delta\sigma^*$. When expressed in terms of the generalized variables, it yields for any element (e):

$$\Delta w_{(e)} = \Delta w^{\text{int}}_{(e)} = \int_{(e)} \langle \Delta\tilde{D} \rangle \{\Delta S\}\, \mathrm{d}V \tag{11}$$

where $\langle \Delta\tilde{D} \rangle$ is the transposed vector of virtual generalized strains. The substitution of Eq. (10) for $\{\Delta S\}$ in the above expression, and the summing for all the finite elements yield:

$$\forall t,\Delta t: \quad \left[\tilde{K}(t)\right]\{\Delta q\} = \{\Delta F^*\} - \left\{F^{\text{his}}(t)\right\} \tag{12}$$

where $\{\Delta q\}$ denotes the increase in the nodal displacements induced during the time interval $[t,t+\Delta t]$. $[\tilde{K}(t)]$ is a fictitious stiffness matrix that accounts for the viscoelastic behaviour of the structure. Its value must be updated at the beginning of every step of time, as follows:

$$\left[\tilde{K}(t)\right] = \sum_{(e)} \int_{(e)} [B]^{\text{t}} \left[\tilde{H}(t)\right][B]\, \mathrm{d}V \tag{13}$$

$[B]$ is the matrix derived from the shape functions, $[B]^{\text{t}}$ being the transposed matrix. The form of $[\tilde{H}(t)]$ is shown in Table 1. The vectors $\{F^{\text{his}}(t)\}$ and $\{\Delta F^*\}$ are a double set of fictitious nodal forces that account for the cumulative effects and for possible free dilation, respectively. They are calculated as follows:

$\forall t,\Delta t$

$$\{\Delta F^*\} = \sum_{(e)} \int_{(e)} [B]^{\text{t}} \{\Delta S^*\}\, \mathrm{d}V$$

$$\left\{F^{\text{his}}(t)\right\} = \sum_{(e)} \int_{(e)} [B]^{\text{t}} \left\{S^{\text{his}}(t)\right\} \mathrm{d}V \tag{14}$$

This formulation has been implemented in the finite element program CASTEM 2000 [6]. The choice of this object oriented program has been preferred because it allows easy implementation of the step-by-step procedure. Classic beam, plate and shell finite elements are used. The original stiffness matrix has been completed in order to take account of the coupling terms shown in Table 1. The calculation of the fictitious nodal forces $\{\Delta F^*\}$ and $\{F^{\text{his}}(t)\}$ is processed by means of an existing routine concerned with thermo-elastic stresses.

The overall algorithm of the complete procedure is described in Fig. 2. A set of cumulative variables $\sigma_\mu(t)$ (see Eq. (4)) is attached to every node of the finite elements. A computation step begins with the calculation of a fictitious modulus $\tilde{E}_i(t)$ for each constituting material. The fictitious stiffness matrix $[\tilde{K}(t)]$ is then updated, and the fictitious nodal forces are calculated (Eq. (14)). The resultion of Eq. (12) yields the incremental increase in the node displacements, to be added to their previous values. Stress and strain increments are then calculated, then added to the previous state of the structure. At the end of the calculation step, the cumulative variables $\sigma_\mu(t)$ are updated according to the actual state of stress at the element nodes.

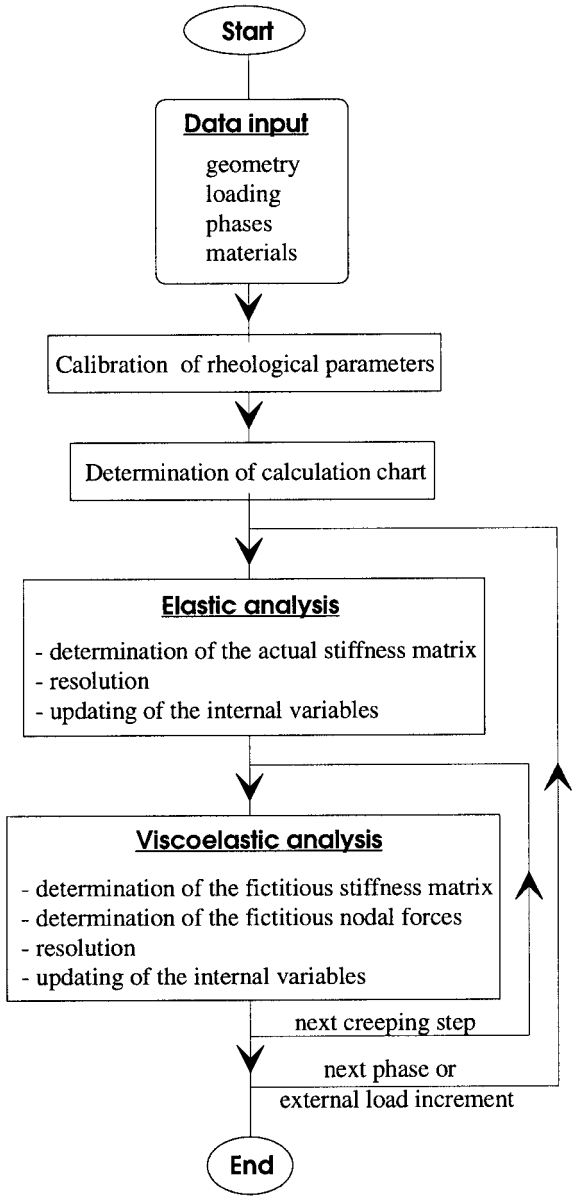

Fig. 2. Overall algorithm of the method.

4.2. Taking account of the process of construction

Engineering structures are generally built sequentially. During the period of construction, the geometry and the weight of the structure is modified with the erection of every new part. Simultaneously, restraint on displacements may be modified, due to a change in the nature, number or location of supports for example. This stepwise evolution of the stiffness, static scheme and dead weight of the structure induces sudden changes in stress distribution and short term displacements. If the behaviour of the constituting materials is time-dependent, these changes may cause a significant redistribution in internal forces and long term displacements during the service life of the structure. As a consequence, the serviceability of the structure can be endangered because of unexpected cracking or excessive deflection, for example.

In order to account for these phenomena, the construction process is divided into elementary stages. One stage corresponds to a modification of the structure or to a change in the loading. The step-by-step procedure presented above is very convenient for taking the construction process into account. The period of construction is described by a chart, where every new construction stage (or loading stage) corresponds to the beginning of a calculation step. Every new stage causes the calculation of an elastic incremental response to be added to the previous state of the structure. This "elastic step" is followed by either one or several viscoelastic calculation steps (Fig. 2). The erection of every new part of a structure cast in place is analysed as two stages: before setting, the wet concrete is accounted for as external loading without modification of the stiffness of the structure; after setting, the global stiffness is modified to account for the contribution of the new part. If the structure is erected in different parts before connection, each part is analysed as independent structure until connection time. The connection corresponds to one specific stage: appropriate condition concerning the relative displacement must be introduced to account for the way of connection. From this time, the two part are analysed as one single structure.

5. Time analysis of real structures

In this section, we present two examples of application of the method to real structures. The former example concerns a prestressed beam tested by other authors [7]. The behaviour of the beam is known over 5 years. This application allows estimation of the validity of our method through a comparison of computed values with test figures. The second application concerns a huge concrete structure (cooling tower) [8]. The numerical analysis gives an estimation of the influence of time effects on the behaviour of the structure. Special attention is paid to the evolution of the stress distribution in the concrete, since excessive tensile stress can lead to unexpected cracking.

5.1. Application to a prestressed concrete beam

We first apply our method to a structural element whose behaviour was previously investigated by Espion and Halleux [7]. The element is a single-span

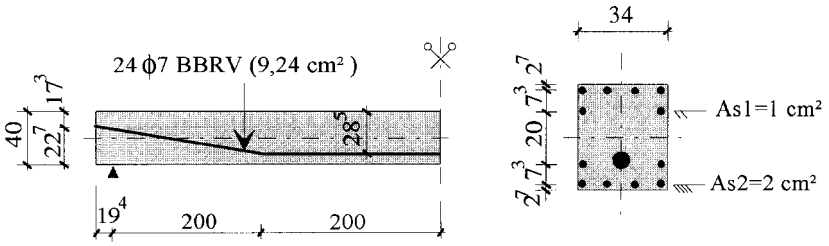

Fig. 3. Definition of the computed beam.

prestressed concrete beam. Its main characteristics are shown in Fig. 3. The beam was subjected to its dead weight and to the prestressing force. No other load was applied to the beam. The record of the time behaviour of the beam is available up to 1843 days (≃5 years). The test figures concern the deflection at given locations along the beam, and the longitudinal strain distribution throughout the depth of the beam at the same locations.

The time dependent behaviour of the concrete was investigated on prismatic samples made of the same concrete mix as in the tested beam. Creep and shrinkage strains were recorded over a 3 year period. Since the samples differed in size from the cross-section of the beam, the test results were corrected to account for size effect. The authors finally fitted two empirical relationships for their experimental data. These expressions represent the creep function and the shrinkage function of the concrete to be used for the tested beam (the values of the coefficient result from the fitting):

$$J(t,t_0) = \frac{1}{26{,}000}\left(1 + 2.867 t_0^{-0.118}\frac{(t-t_0)^{0.6}}{15+(t-t_0)^{0.6}}\right) \quad (15)$$

$$\epsilon_{sh}(t) = -0.48\times 10^{-3}\frac{t}{78+t} \quad (16)$$

where t,t_0 in days, $J(t,t_0)$ in MPa^{-1}.

The beam was post-tensioned 45 days after casting. At prestressing, the force in the tendon was adjusted in order to obtain a longitudinal strain equal to zero at the uppermost fiber at mid-span of the beam. According to the authors, the initial stress in the tendon was equal to 1200 MPa. The relaxation loss after 1000 h is estimated equal to 1.5% of initial stress. Intermediate values are required in order to calibrate the coefficients in Eq. (3). Since no more information is given by the authors concerning the evolution of relaxation loss in terms of time, we decide to fit Eq. (3) for the figures proposed by Eurocode 2 [1,2]. As a result of the calibration, the relaxation function of the tendon may be represented by the following Dirichlet series:

$$R(t,t_0) = 191.8 + 6.6e^{-\frac{t-t_0}{4000}} + 1.6e^{-\frac{t-t_0}{25}} \quad (17)$$

(in GPa)

Taking advantage of the symmetry, only the other half of the beam is meshed for the finite element analysis. All composite beam elements are given the same length. The characteristics and locations of the reinforcing bars and the prestressing tendon are included in every element, according to the method described above. Where the tendon is not horizontal, its location is given the value of the eccentricity at mid-length of the element. The tensioning of the tendon is simulated as a self-contraction of the steel. Creep and shrinkage of the concrete and stress relaxation in the prestressing device, are taken into account during the calculation.

Preliminary calculations show that eight finite elements are sufficient to ensure the accuracy of the results. The life span of the beam is divided into computation steps progressively increasing in length. With such a method, only 13 steps are necessary to scan the structure life (5 years) with a good accuracy.

Computed and experimental values of the generalized strain components at mid-span of the beam are plotted on the next figures. The predicted values of the axial strain are quite satisfactory during the first year of creeping (Fig. 4). Then they diverge progressively from the test figures. The final difference is about 10% after 5 years. Concerning the curvature, a significant difference is observed between the computed values and the test figures (Fig. 5). Similarly, the predicted evolution of the mid-span deflection is compared with the published values on Fig. 6. Although the two lines are similar in shape, the computation under-estimates the real deflection of the beam by about 24%. Actually, the behaviour of the beam is very sensitive to the features of the prestressing (initial force, eccentricity). As a matter of fact, the exact position of the tendon in the duct is not known exactly, only estimated. A complementary computation (dashed line on Fig. 6) shows that an error of 1 cm on the eccentricity of the

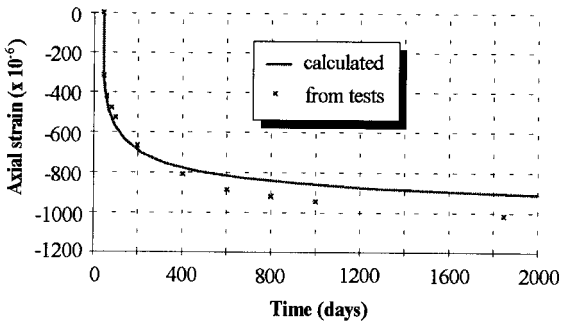

Fig. 4. Evolution of the axial strain at mid-span.

tendon can explain about 60% of the total difference between computed and experimental values. This correction has no significant influence on the computed axial strain (Fig. 4).

The computation provides valuable informations about the evolution of the state of stress in the structure. On Fig. 7, the repartition of the stresses in the mid-span cross-section is shown at three different times. A progressive decrease in stress is observed in the prestressing steel and in the concrete. Simultaneously, the compressive stresses increase in the passive reinforcement (from 140 to 306 MPa in the lowermost bars, from 46 to 123 MPa in the uppermost one). Most of the total decrease in the prestressing stress (about 18% after 5 years) is caused by the creep and shrinkage of the concrete. Less than a quarter of the stress decrease results from relaxation.

5.2. Application to the time analysis of a cooling tower

The structure is an axi-symmetric shell made from reinforced concrete (Fig. 8). Its inner diameter varies between 121.1 m at the base and 83.3 m at the altitude of 163.9 m. The shortest diameter, at the neck of the tower, is 77 m at the altitude of 127 m. The shell is supported by 50 pairs of reinforced concrete columns.

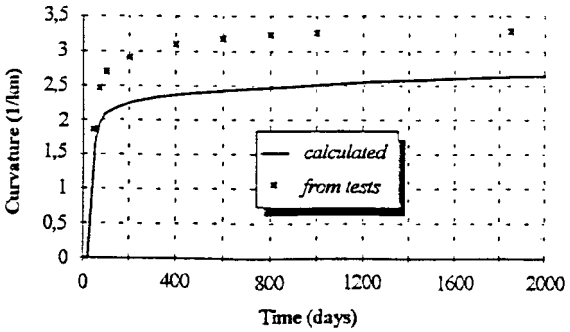

Fig. 5. Evolution of the curvature at mid-span.

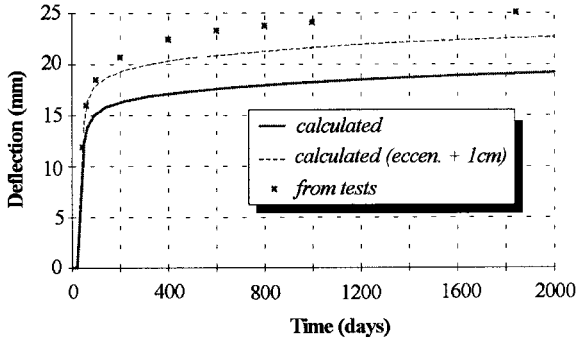

Fig. 6. Evolution of the deflection at mid-span.

It is crowned at its top with a visit gallery. The overall height of the tower is 165 m.

The thickness of the shell varies between 21 and 32 cm over the most of the structure. The radius R_m of the middle surface of the shell can be expressed in terms of the altitude z as follows (z and R_m in meters):

$$R_m = 23.333 - 0.00263z + 0.2986\sqrt{(z - 126.74)^2 + 2694.5} \quad (18)$$

The shell is reinforced by a double net of ribbed bars disposed orthogonally on each face, with a concrete cover of 2.5 cm. The diameter of the bars varies between 10 and 16 mm. The ratio of reinforcement is more or less uniform for the all structure. Compared with the concrete cross-section, the ratio is about 0.40% (0.20% on each face) in the horizontal direction, and 0.16% (0.08% on each face) in the vertical direction.

Close to the base, the thickness of the shell is enlarged to 120 cm in order to shape a rigid annular beam. The reinforcement described above is completed with hoop bars (20 ribbed bars/diameter 25 mm) and with closed stirrups.

Similarly, the thickness of the shell is enlarged to 92 cm beneath the visit gallery. The horizontal reinforcement is completed with 28 ribbed bars, diameter 25 mm.

Ordinary concrete was used for the construction. The concrete was made of Portland type cement, class 400, the cement content being 350 kg/m^3. The mean compressive strength at 28 days was about 36.4 MPa. During the construction, the shell was divided into 62 horizontal rings, with a constant height of 2.60 m for most of them. Each day, the form was lifted up and adjusted, then the next ring was cast.

We assume that the evolution of creep and shrinkage of the concrete may be described by the functions proposed by Eurocode 2 [1,2]. According to this standard, both the creep and the shrinkage functions

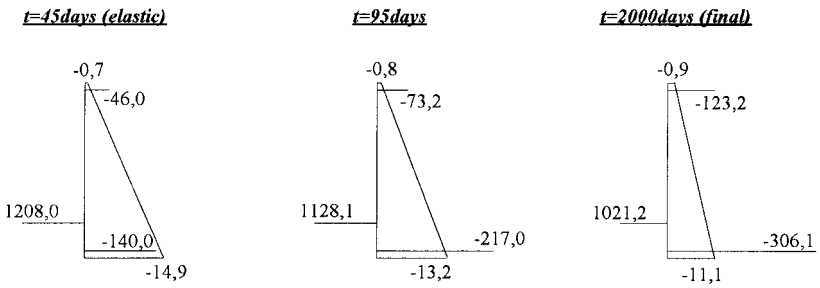

Fig. 7. Evolution of the stress distribution in the middle cross-section (MPa).

depend on the notional size h_0 of the element and the relative humidity ρ_H of the ambient atmosphere. For the calculation, these parameters are given the following values: $h_0 = 0.34$ m (average thickness of the shell), $\rho_H = 0.70$. Besides these two parameters, the creep function depends on the time t_0 at first loading, the mean compressive strength of the concrete and the type of cement. According to our method, the relaxation function is derived from the creep function of different values of t_0, then expanded into Dirichlet's series as expressed by Eqs. (3) and (9).

For the numerical analysis, the shell is represented by 62 axi-symmetric finite elements, corresponding to the 62 elementary rings mentioned above. Each finite element is given a uniform thickness corresponding to the average thickness of the relevant ring. Only the shell is concerned with the FEM analysis. Appropriate limit conditions must be introduced at the lowest edge of the shell: optional restraint may be imposed on the vertical displacement (u_z), the radial displacement (u_r) and the rotation (r_t). Fig. 9 shows the effects of various limit conditions on the displacement of the middle surface of the shell as they result from elastic calculations (displacement magnification is 3500:1). It is seen that restraining the rotation has no decisive effects on the computed values. As a matter of fact, a closer investigation shows that there is no significant bending effect in this region of the shell.

The question of the radial displacement is more crucial. The internal forces at the base of the shell are collected by the annular beam described above, then transmitted to the footing of the structure by the columns. Bearing in mind that the angle of inclination of the columns is equal to the slope of the shell at its lowest edge, it can be assumed that the state of stress in the columns is close to pure compression. This assumption is consistent with the previous conclusion concerning the rotation. Therefore, the flexibility of the columns may be omitted. As a conclusion, we decide to restrain the vertical displacement and the radial displacement at the base of the shell, whereas the rotation is kept free.

To complete this discussion, a comparative calculation with various curvature values for the shell meridian has been performed (u_z and u_r restrained). Results corresponding to four cases going from a cylindrical shell (line 1) to the actual geometry (line 4) are shown in Fig. 10 (thickness distribution in terms of the altitude has been preserved). It is seen that the radial dis-

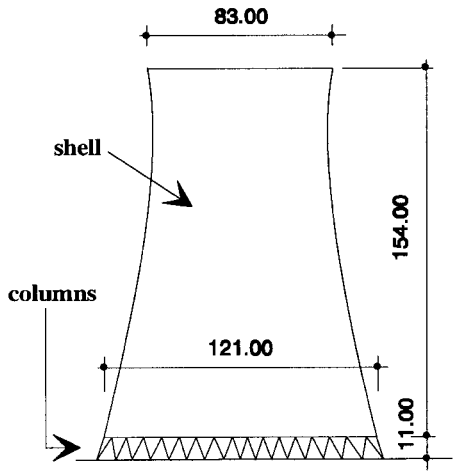

Fig. 8. Overall view of the cooling tower.

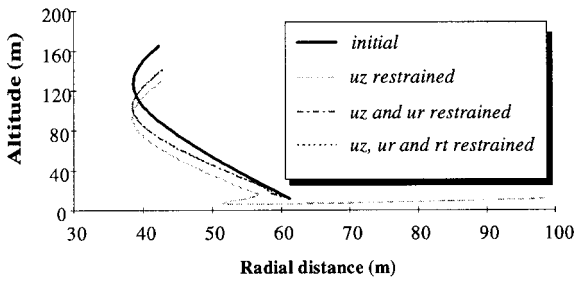

Fig. 9. Influence of the limit conditions at the base ("elastic" calculation).

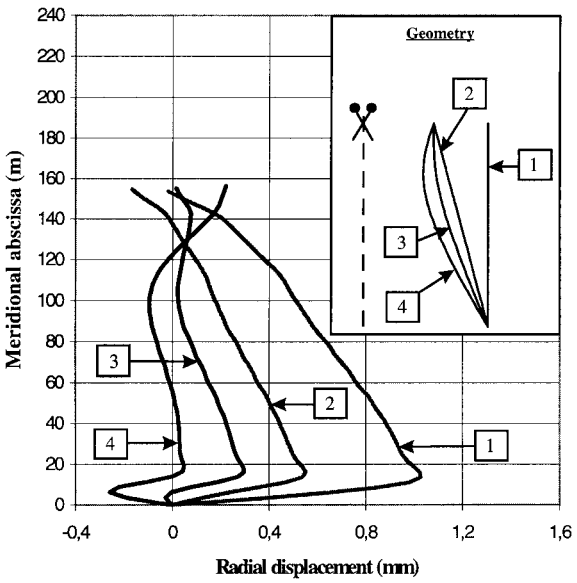

Fig. 10. Influence of the meridional curvature on the radial displacement ("elastic" calculation).

placement pattern is strongly related to the meridional curvature of the shell, especially in the lower region.

The time analysis of the shell is conducted as follows. Every day, the mould is removed and lifted up by one element height. The top of the mould is adjusted in order to meet the theoretical geometry of the shell. After casting, the weight of the mould and the weight of the fresh concrete are supported by the older part of the structure. To take account of this method of construction, the numerical procedure is divided in one elastic computation followed by one or several viscoelastic steps. The weight of the new ring is accounted for by a force applied to the upper node of the last-built element. The new ring does not contribute to the stiffness of the structure until the next day. After each computation step (elastic or viscoelastic), the state of the already-built part of the structure is updated in order to take the incremental increase in stresses, strains and displacements into account. The next day, the mould is removed and the new ring becomes part of the structure. All state values attached to the upper node of the new element are given zero values. This cycle is undertaken 62 times in order to scan the whole process of construction of the shell. The computation corresponding to the period of construction is followed by a number of viscoelastic computation steps, in order to complete the time analysis of the structure over a 30 year life span (≃11,000 days).

Fig. 11 shows the evolution of the radial displacement as resulting from the computation process

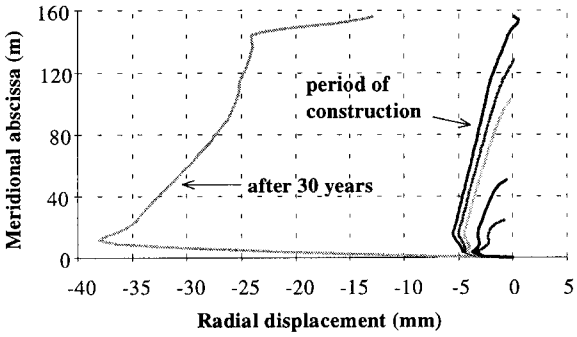

Fig. 11. Radial displacement ("viscoelastic" calculation).

described above. Negative values correspond to a diminution of the radius of the shell. During the construction, the uppermost edge of the shell is constantly adjusted to its theoretical position, as mentioned above. This is the reason why the displacement amplitude remains rather small during the period of construction, compared with the size of the structure. The radial displacement increases considerably during the next 30 years.

The long term displacement pattern can be qualitatively compared with the displacement pattern resulting from elastic analysis (curve 4 on Fig. 10). Obviously, the computed values are quite different in their distribution in terms of the altitude. Fig. 12 gives an explanation of this difference. The short term displacement pattern depends on the process of construction (curve

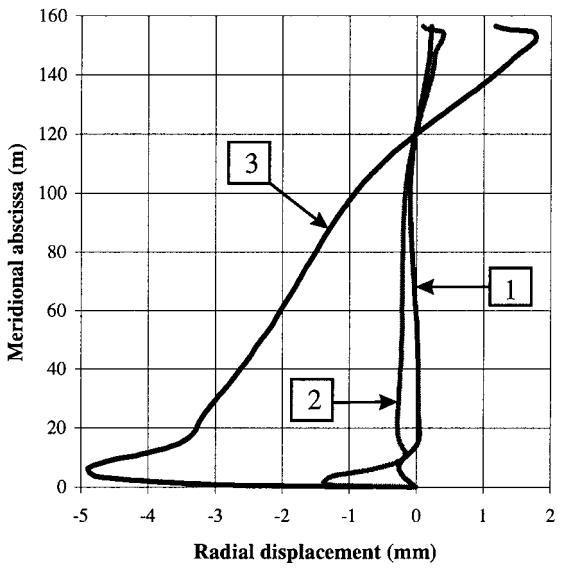

Fig. 12. Radial displacement: line 1, elastic; line 2, elastic (incremental construction); line 3, viscoelastic (shrinkage omitted).

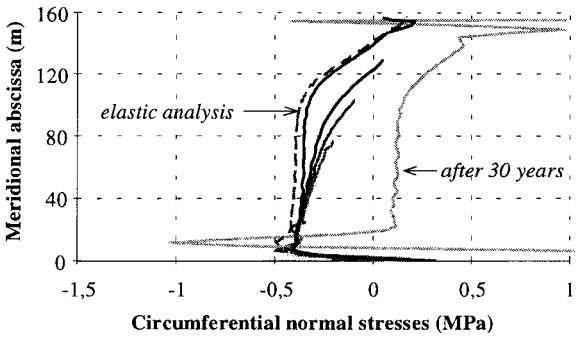

Fig. 13. Distribution of the hoop stress in concrete.

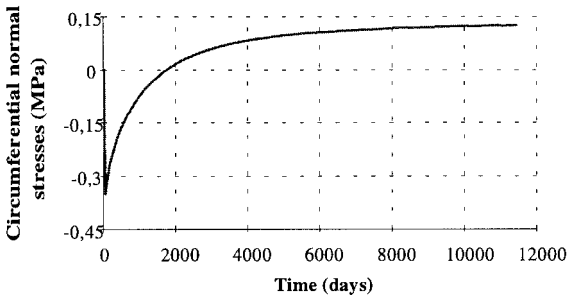

Fig. 14. Evolution of the hoop stress in concrete.

2 versus curve 1). Taking the phases of construction into account, the elastic analysis and the long term analysis (without shrinkage) yield qualitatively similar patterns (curve 2 versus curve 3). The final diagram on Fig. 11 is similar in shape to curve 3 on Fig. 12: the difference in magnitude results from the effects of shrinkage. This discussion shows that the long term behaviour of such a structure depends on any time-related parameter, including the process of construction.

The model gives access to the stress distribution in the concrete and in the reinforcing steel within any cross-section of the structure. Fig. 13 shows the evolution of the hoop stress in the concrete, close to the outer surface of the shell. It can be seen that the concrete remains compressed during the period of construction.

Then the compressive stress decreases progressively and turns to tension after a few years. This evolution is shown in Fig. 14 for a point located at an altitude about 80 m. After 30 years, the distribution of the tensile stress is about uniform ($\simeq$0.13 MPa) in the lower half of the tower. It is interesting to notice that the existence of tensile stresses cannot be predicted from an elastic computation (dashed line on Fig. 13). Still, reliable information is required about the state of stress in order to estimate the risk of cracking, especially in the lower part of the tower where temperature conditions are worse.

6. Conclusion

The method presented above is based on the theory of linear viscoelasticity. It applies to composite structures made of elastic or viscoelastic materials, such as wood, concrete, reinforcing or prestressing steel, etc. The efficiency of the method originates from the combination of an incremental approach to account for time effects, with a global approach to express the behaviour of usual structural elements in terms of the generalized variables of the beam, plate or shell theories.

The method allows to predict the consequences induced by time dependent effects in composite structures. Changes in the stress and strain distribution, and progressive deflection of the structure, can be analysed, taking account of the way of construction and the time dependent behaviour of the constituting materials. The numerical figures may differ substantially from those obtained from an elastic analysis. By using this method, it is possible to predict the range of stress redistribution or to evaluate long term deflection in huge or complicated concrete structures for example.

References

[1] Eurocode 2. Design of concrete structures, part 1, ENV 1992-1, CEN 1991.
[2] Destrebecq JF. Rheology of concrete building materials according to Eurocode 2. In: Proceedings of the international Conference on Selected Design Problems of Concrete Structures According to Eurocode 2, Cracow, 16–17 June, 1994. p. 23–36.
[3] Bazant ZP, Carol I. Preliminary guidelines and recommendations for characterizing creep and shrinkage in structural design codes. In: Creep and shrinkage of concrete. London: Spon, 1993. p. 805–30.
[4] Salencon J. Viscoélasticité. Paris: Presses de l'Ecole Nationale des Ponts et Chaussées, 1983.
[5] Bazant ZP, Wu ST. Rate type creep law of aging concrete based on Maxwell chain. Mater Struct 1974;37:45–60.
[6] CASTEM 2000 Logiciel de calcul par éléments finis, CEA-CEN Saclay, France 1996.
[7] Espion B, Halleux P. Long term behavior of prestressed and partially prestressed concrete beams: experimental and numerical results. In: ACI-SP129 Computer analysis of the effects of creep, shrinkage and temperature changes on concrete structures, 1991. p. 19–38.
[8] Destrebecq JF, Ghazlan G, Jurkiewiez B. Evaluation des effets due fluage dans un aéroréfrigérant atmosphérique. Rapport de contrat ND 2437 MS, EdF, Direction de l'équipement 1995.